

Excitonic Coupling and Photon Antibunching in Venus Yellow Fluorescent Protein Dimers: A Lindblad Master Equation Approach

Ian T. Abrahams 

Quantum Biology Doctoral Training Centre
University of Surrey, Guildford GU2 7XH, United Kingdom
i.abrahams@surrey.ac.uk

Abstract

Strong excitonic coupling and photon antibunching have been observed together in Venus yellow fluorescent protein (YFP) dimers—a cryptic combination under prevailing theoretical models. In 2019, Kim *et al.* demonstrated Davydov splitting in Venus dimer circular dichroism (CD) spectra, revealing large negative dimer coupling energy, while antibunching was confirmed by antibunching–fluorescence correlation spectroscopy (AB/FCS fingerprinting). To explain this coexistence, Venus dimer population dynamics are modeled here within a Lindblad master equation framework, justified by the separation of characteristic coupling, dephasing, and thermal relaxation rates. Simulations predict rapid decoherence, consistent with antibunching, indicating that coherence in both the excitonic and site bases is too short-lived to affect photon emission statistics. Despite the absence of long-lived coherence, Venus dimers provide a tractable platform for probing evolutionary pressures on fluorescent protein photophysics and quantum dynamics. Cryogenic cooling could extend coherence lifetimes into the regime required for quantum gate operations, suggesting a route toward fluorescent protein–based qubits. More broadly, the results highlight a structural design principle—a “bioexciton motif”—that links excitonic coupling, decoherence, and protein architecture, pointing to general rules by which biology both constrains and inspires quantum technologies.

I Introduction

Like Brownian motion before it, the Venus dimer presents an experimental puzzle demanding a theoretical explanation [1, 2, 3]. In 2019, Kim *et al.* revealed Davydov splitting in Venus dimer circular dichroism (CD) spectra, indicating strong excitonic coupling, with a negative coupling energy value, alongside a small, associated redshift in absorption peak following Venus dimerization. Photon antibunching was also observed in Venus dimers, using their own antibunching–fluorescence correlation spectroscopy technique (AB/FCS fingerprinting) [2]. This coexistence can be perceived as cryptic, given that under prevailing models, strongly coupled molecular dimers which sustain excitonic coherence in the energy basis tend to exhibit bunched superradiance [4]. Instead, Venus dimers behave as single quantum emitters, indicating that coherence in both site and excitonic bases is too short-lived to influence emission statistics.

Earlier modeling of green fluorescent protein (GFP) dimers, such as Burgess and Florescu’s analysis of decoherence and dielectric relaxation [5], underscore the importance of bath dynamics but do not resolve the coexistence of strong coupling and antibunching at room temperature. No framework has yet underscored the precise mechanism underlying the interplay between coupling strength, spectral shifts, and photon statistics as observed by Kim *et al.*. Here, I address this gap by developing a Lindblad master equation framework, justified by the clear separation of derived characteristic coupling, dephasing, and thermal relaxation rates.

This analysis reconciles strong excitonic coupling with photon antibunching and the observed absorption redshift, predicting rapid decoherence consistent with experimental results. It also suggests that cooling Venus dimers to the 10–100 mK regime [6] could extend coherence lifetimes into the range required for quantum gate operations, positioning fluorescent protein dimers as candidate qubits. More broadly, the

results highlight a structural design principle—a “bioexciton motif”—linking excitonic coupling, decoherence, and protein architecture and pointing to general rules by which biology both constrains and inspires quantum technologies.

II Open Quantum Systems Model

II.1 Excitonic Basis and Hamiltonian

Let $|1\rangle$ and $|2\rangle$ denote localized excitations of two chromophores. In the strong-coupling regime these combine to form delocalized excitonic states,

$$|+\rangle = \frac{|1\rangle + |2\rangle}{\sqrt{2}}, \quad |-\rangle = \frac{|1\rangle - |2\rangle}{\sqrt{2}}, \quad (1)$$

corresponding to the bright (symmetric) and dark (antisymmetric) states. Such coherent superpositions of localized excitations are described in standard treatments [7] and reflect the broader perspective of Scholes [8], who emphasized the central role of delocalization and coherence in molecular excitonic systems.

The Hamiltonian in this basis is diagonal with eigenenergies

$$E_{\pm} = \bar{\varepsilon} \pm \frac{1}{2}\Delta E, \quad \Delta E = \sqrt{\Delta^2 + 4J^2}. \quad (2)$$

For a homodimer ($\Delta = 0$), $\Delta E = 2|J|$, so that $E_{\pm} = \bar{\varepsilon} \pm J$. For negative coupling ($J < 0$), the bright state $|+\rangle$ lies lower in energy than the dark state $|-\rangle$, consistent with the dephasing and relaxation derivations in Appendix A. Such delocalization is, however, strongly limited by disorder and thermal fluctuations, as emphasized by Scholes in an independent publication [9].

II.2 Lindblad Formalism

The reduced system density operator $\hat{\rho}(t)$ is evolved using a Lindblad master equation in the Born–Markov–secular approximation [10],

$$\frac{d\hat{\rho}}{dt} = -\frac{i}{\hbar}[\hat{H}, \hat{\rho}] + \sum_{l \in \{\phi, -, +, +-\}} \mathcal{L}(\hat{\rho}, \gamma_l), \quad (3)$$

where γ_{ϕ} is the pure-dephasing rate, while γ_{-+} and γ_{+-} are the downhill and uphill thermal transfer rates, respectively. Explicit derivations of these expressions are given in Appendix A. The bath correlation parameters that determine these rates, namely the cutoff frequency γ_c , and the effective reorganization energy λ , were extracted from experimental coherence times of GFP reported by Cinelli *et al.* [11] and the dielectric relaxation model of Burgess and Florescu [5].

II.3 Thermal Dynamics with Stokes Shift

Following solvent and protein relaxation, a site-energy difference Δ (Stokes shift) is introduced. The resulting generalized site-basis Hamiltonian is

$$\hat{H} = \begin{bmatrix} -\Delta/2 & J \\ J & +\Delta/2 \end{bmatrix}, \quad (4)$$

where Δ is the site-energy difference after relaxation. The corresponding exciton splitting is

$$\Delta E = \sqrt{\Delta^2 + 4J^2}, \quad (5)$$

so that the eigenenergies are $E_{\pm} = \bar{\varepsilon} \pm \frac{1}{2}\Delta E$. For $J < 0$ and parallel site dipoles, the lower exciton is bright, and thermal relaxation produces a strong bias toward this state.

III Results and Discussion

Numerical simulations of open quantum systems were performed using QuTiP v5.2.0 [12, 13], with supporting scientific computing provided by NumPy v2.3.2 [14] and SciPy v1.16.0 [15].

III.1 Photon Antibunching and Subpicosecond Dynamics

We analyze photon antibunching and subpicosecond (sub-ps) dynamics in Venus dimers. Using Venus-like parameters: $J = -34$ meV, $T = 293$ K, and an effective reorganization energy $\lambda = 2.7 \times 10^2 \text{ cm}^{-1} \sim 34$ meV $\sim |J|$, with bath cutoff γ_c , as defined in Section II from Cinelli *et al.* [11] and Burgess & Florescu [5]. Near-resonant value for J and λ suggest an intermediate regime where coupling is strong and decoherence is rapid [16].

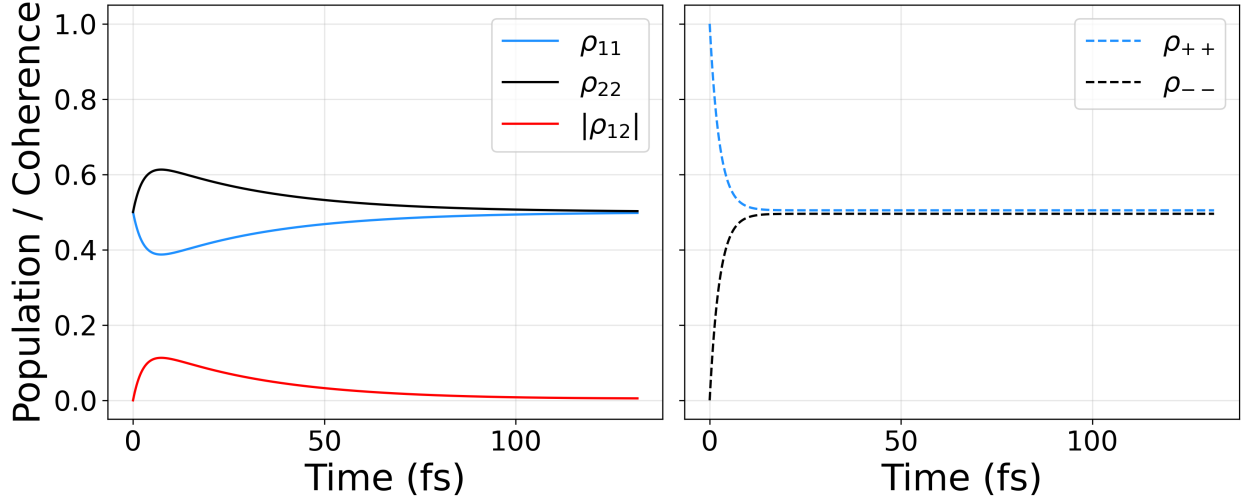


Figure 1: **Room-temperature, sub-ps dephasing and thermal relaxation dynamics.** Time evolution of exciton populations and coherences for a Venus-like homodimer with $J = -34$ meV at $T = 293$ K. **Left:** site-basis populations ρ_{11} and ρ_{22} with coherence magnitude $|\rho_{12}|$, initialized in a 50:50 superposition with phase factor $\phi = \pi/2$. **Right:** energy-basis populations ρ_{++} and ρ_{--} following bright-state initialization. In this homodimer case ($\Delta = 0$), the exciton splitting is $\Delta E = 2|J|$, and dynamics are dominated by thermal relaxation and dephasing at room temperature.

The expectations for this regime are consistent with results shown in Figure 1. In the homodimer limit ($\Delta = 0$), the exciton splitting is $\Delta E = 2|J|$, giving eigenenergies $E_{\pm} = \bar{\epsilon} \pm J$. In this case, the pure-dephasing rate

$$\gamma_{\phi} = \frac{2 \lambda k_B T}{\hbar^2 \gamma_c}$$

yields critically damped population dynamics: $\rho_{11}(t)$ and $\rho_{22}(t)$ relax monotonically with a quickly decaying $|\rho_{12}(t)|$. In the energy basis, populations approach an equal ($\sim 50:50$) mixture within tens of femtoseconds, consistent with rapid decoherence between excitons under these conditions. This explains why Venus dimers act effectively as single emitters at room temperature despite strong coupling [2].

Furthermore, the relatively small observed spectral redshift (~ 0.9 nm) juxtaposed with the sizeable $|J| = 34$ meV means the “bright-state” energy predicted by strong coupling is not cleanly resolved in ensemble spectra—naturally explained if emission averages over a mixture of localized bright and dark character as the system rapidly dephases.

III.2 Thermal Dynamics from a Mixed State

After sub-ps relaxation, initializing a 50:50 bright-dark mixture yields a strong thermal bias toward the bright exciton ($\gtrsim 0.97$ population at 293 K) (Figure 2). This thermal funneling explains why, despite rapid decoherence, emission statistics remain dominated by the bright state at room temperature. Such a bias offers a mechanistic underpinning for the enhanced brightness observed in Venus dimer variants.

Kim *et al.* directly observed this effect in their tandem-dimer construct Venus_{A206}-TD [2]. In their Figure 5, time-resolved anisotropy measurements showed a dramatic reduction in limiting anisotropy relative to monomeric Venus_{A206K} (panel A), consistent with ultrafast energy transfer and rapid equilibration into the

bright state. Brightness analysis (panel B) revealed that Venus_{A206}-TD emitted with nearly twice the photon output of a monomer, as expected for a coherent dimer in which emission is thermally biased toward the lower, bright exciton, while a control construct with widely separated fluorophores (Venus_{A206K}-20nm-TD) displayed an apparent slight decrease in brightness.

Additionally, photon antibunching traces (panel C) demonstrated that Venus_{A206}-TD behaved as a single-photon emitter, with a center-to-side (C/S) coincidence ratio indistinguishable from the A206K monomer. The AB/FCS fingerprint (panel D) confirmed this interpretation: Venus_{A206}-TD followed the single-emitter line, while a control construct with widely separated fluorophores (Venus_{A206K}-20nm-TD) displayed elevated C/S ratios indicative of increased independent emission of its site chromophores.

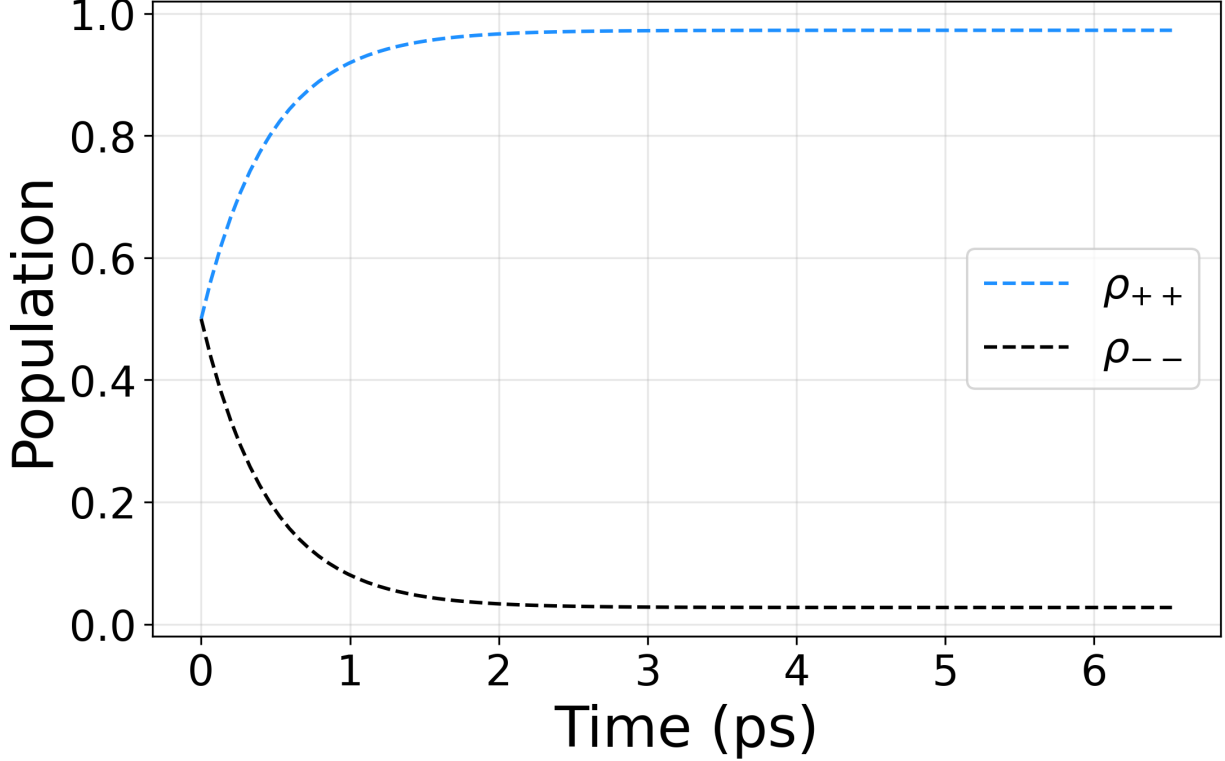


Figure 2: **Population relaxation from an equal bright-dark mixture.** energy-basis population dynamics for a Stokes-shifted Venus-like dimer with $\Delta = 59.28$ meV and $J = -34$ meV at $T = 293$ K. The exciton splitting is $\Delta E = \sqrt{\Delta^2 + 4J^2} \approx 90.2$ meV. Thermal transfer favors the bright exciton, ρ_{++} (blue, dashed), leading to biased steady-state emission.

Together, these observations validate the framework prediction: thermal relaxation heavily favors the bright exciton, so strongly coupled Venus dimers appear both brighter than monomers and yet antibunched, as though they were single quantum emitters. This underscores the sensitivity of J to dipole geometry and provides an experimental benchmark for linking excitonic structure to brightness, as previously explored in anisotropy-decay comparisons of A206K Venus variants [2]. Having established this correspondence between model and experiment, it is natural to ask what new experiments and theoretical approaches could further probe and extend this picture.

III.3 Future Work: Experimental and Theoretical Directions

Building on this framework, several experimental and theoretical avenues suggest themselves. On the experimental side, cryogenic antibunching combined with fluorescence correlation spectroscopy (AB/FCS fingerprinting) [2] could directly test whether coherent superpositions in the excitonic basis can be stabilized at reduced temperatures, revealing superradiant signatures that remain hidden at room temperature [4].

Finite detector resolution still limits the observation of ultrafast superradiant photon-bunching features, but advances in time resolution will be decisive for probing such regimes.

On the theoretical side, refined simulations—spanning quantum mechanics/molecular mechanics (QM/MM), molecular dynamics (MD), and time-dependent density functional theory (TDDFT)—can dissect the structural origins of excitonic coupling, clarifying when PDA remains valid [4] and when explicit treatments such as TrESP become necessary [17]. Moving beyond the present Lindblad framework will require approaches capable of treating non-Markovian dynamics [5], correlated baths, and vibrational coherences—such as path-integral techniques [18], hybrid QM/MM dynamics [19], or generalized open-quantum-system formalisms [20].

Ultimately, progress will depend on close interplay between experiment and theory. On the experimental side, new measurements will sharpen the limits of PDA by directly testing how brightness differences track structural variation across temperature, dimer interface, and tandem-dimer linker design.

In particular, cryogenic antibunching experiments could provide decisive tests of whether single-emitter statistics persist when coherence lifetimes are extended, while ultrafast spectroscopies (e.g. 2DES) can probe vibronic coherence and energy transfer pathways on femtosecond timescales. Such approaches would complement each other in resolving ambiguities that have long complicated the interpretation of coherence in complex systems such as photosynthetic light-harvesting complexes [21, 3]. On the theoretical side, refined models will not only clarify when explicit charge-based approaches such as TrESP are required, but also provide a framework for testing broader assumptions about bath response, coherence lifetimes, and mechanisms of bright-state selection. Together, these advances will link fluorescent protein excitonics to structural motifs that illuminate both principles of biological adaptation and strategies for designing molecular qubits with tunable coherence, simultaneously contributing to the emerging field of quantum biophotonics.

IV Extended Discussion

The results above establish a mechanistic framework for reconciling photon antibunching, strong excitonic coupling, and spectral shifts in Venus dimers. Beyond this specific model, however, lies a broader principle: excitonic behavior in fluorescent protein scaffolds appears to be both an evolutionary adaptation and a technological opportunity. Structural conservation across *Aequorea* spp. fluorescent proteins suggests that selective pressures have acted on relative chromophore geometry (roughly C_2 -symmetric [22]), protonation equilibria, and oligomerization, analogously to known photosynthetic light-harvesting complexes (e.g. C_3 -symmetry in the Fenna-Matthews-Olson light-harvesting complex from *Prosthecochloris aestuarii* green sulphur bacteria) [23, 24], hinting at a recurring biological design principle—the “bioexciton motif” that stabilizes optical function across species and environments.

The fundamental unit of this motif is the chromophore dimer—biological chromoproteins appear pre-disposed to oligomerize, stabilizing and optimizing structure-function relationships within the constraints of their evolutionary history. Elucidating these symmetries and any random or systematic deviations from them more precisely may enable the development of simplified chromoprotein models within a unifying framework, tying together structural and functional relationships across diverse evolutionary lineages. Simultaneously, the same motif provides a template for engineering excitonic qubits and coherent photonic devices, where the interplay of coupling, decoherence, and structural architecture can be deliberately tuned. These dual perspectives—evolutionary (Section IV.1) and technological (Section IV.2)—highlight how a single physical mechanism can bridge natural adaptation and quantum design.

IV.1 Evolutionary Implications

Molecular graphics and analysis were performed using open-source PyMOL (version 2.5, commit d24468af) [25], available at <https://github.com/schrodinger/pymol-open-source>.

The PyMOL alignment (Figure 3) shows strong structural conservation between Venus (1MYW) and wild-type *A. victoria* GFP (1GFL), including the chromophore axis orientation within the β -barrel—important because excitonic coupling and brightness in dimers are acutely geometry dependent. The GFP crystal structure shown reflects typical, rough C_2 -symmetry expected from FP weak dimers [22]. This conservation supports using Venus/GFP as a tractable scaffold to reason about naturally occurring *Aequorea* fluorescent proteins (FPs).

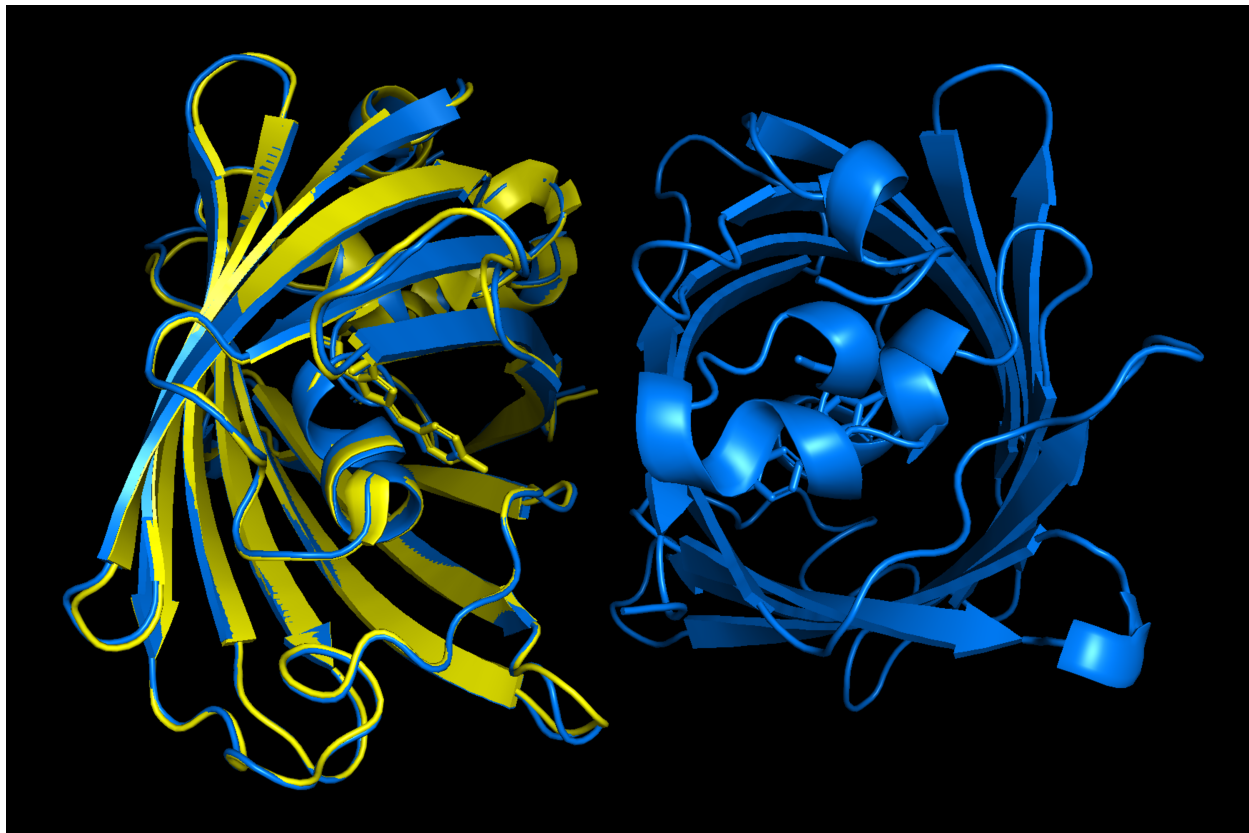


Figure 3: **Structural homology of Venus YFP and wild-type GFP.** Global alignment of cartoon crystal structures of the Venus YFP subunit (yellow; PDB ID: 1MYW) and wild-type GFP dimer (marine blue; PDB ID: 1GFL) (RMSD (\AA): 0.323), highlighting conserved chromophore orientation relative to the β -barrel scaffold. Chromophores are shown as sticks. The roughly- C_2 -symmetric quaternary structure of the GFP dimer is shown.

Recent cloning and spectroscopy across *Aequorea* spp. uncovered diverse paralogs with absorption from blue-green into the far-red, including unusually bright-green FPs and non-fluorescent chromoproteins (CPs) [26, 27]. For *A. cf. australis*, the authors also identified a close avGFP-like ortholog, AausGFP—here nicknamed the *jade fluorescent protein* (JFP) for its slightly blueshifted green emission, distinguishing it from the canonical GFP from *A. victoria*. (Here, JFP is to AausGFP as GFP is to avGFP.) *A. victoria* itself also expresses multiple paralogs, including AvicFP1, the most closely related paralog to both GFP and JFP [26]. Notably, AvicFP1 (along with other related homologs) exhibits a single anionic absorbance peak at 481 nm (no 395/398 nm neutral peak), implying a fully anionic ground state; by contrast, GFP and JFP (formerly AausGFP) display the canonical neutral/anionic dual peak ($\sim 400/480$ nm), which may be an adaptive trait, conserved through speciation, due to the relatively high stability of the neutral chromophore form in the ground state, potentially explaining why AvicFP1 lacks an obvious ortholog [26, 28].

Signaling and BRET constraints. A classic retrodictive hypothesis is that *A. victoria* GFP’s spectra are constrained by the need to accept bioluminescent energy from their native bioluminescence resonance energy transfer (BRET) donor, aequorin (peak emission ~ 475 nm) and to emit green underwater as a behavioral signal. The 477–503 nm (anionic absorption–emission) path supports efficient aequorin→GFP energy transfer; AvicFP1’s $\lambda_{\text{abs}} \approx 481$ nm may offer even tighter, more adaptive, spectral overlap with aequorin (if co-expressed, which they are not [26]) compared to avGFP’s 477 nm band, albeit with potential trade-offs in chromophore stability [29, 28]. Efforts towards modeling and experiments accounting for fully realistic aequorin-GFP fusion complexes serve as a necessary step in testing the presented adaptive hypotheses. Such investigations may explain any apparent discrepancies in expectations in isolated studies of wild-type GFP dimers, and are also expected to apply to wild-type JFP dimers.

Tetramers and higher-order coupling. Additional reef coral and cephalochordate homologs—including DsRed from *Discosoma* and the ancestral cephalochordate LanYFP—exist as obligate tetramers or higher-order aggregates [30, 31]. Structural analyses of DsRed show orthogonal 222 symmetry, chromophore-chromophore separations of 22–43 Å, and dipole orientations that enable efficient intratetramer FRET and rapid depolarization dynamics [30]. Similarly, modeling of LanYFP revealed tetrameric interfaces that had to be disrupted to yield monomeric mNeonGreen [31]. These findings highlight how oligomerization not only redshifts spectra via extended chromophore conjugation but also provides built-in pathways for excitonic/electronic coupling.

Within *Aequorea*, natural paralogs may form higher-order assemblies beyond dimers, raising the possibility that coupling, coherence lifetimes, and functional roles differ systematically across ecological niches and evolutionary lineages. In the context of Venus, such higher-order designs suggest clear engineering routes: tetramerization could be harnessed, alongside tandem-linker design, to stabilize specific dipole geometries, extend coherence through redundant coupling pathways, or bias exciton manifolds toward bright or dark states depending on intended applications. Exploring engineered FP oligomers alongside natural tetrameric homologs may therefore reveal a broader design space where coupling strength, spectral tuning, and quantum coherence are jointly optimized, leading to potential technological advancements currently waiting to be made.

IV.2 Technological Implications for Quantum Computing

For an FP dimer with $|J| = 34$ meV, the coherent beat period is set by the exciton splitting:

$$T_{\text{beat}} \approx \frac{2\pi\hbar}{2|J|} \sim 60 \text{ fs}$$

with a coherence half-life of ~ 30 fs. Scaling to multi-qubit systems requires that coherence half-lives $t_{1/2}$ comfortably exceed gate times T_{gate} by at least an order of magnitude [32, 33], so that errors do not accumulate catastrophically as qubit counts grow. Thus, any gate that leverages excitonic phase (i.e. quantum coherence) must operate on $\mathcal{O}(10\text{--}100)$ fs timescales. At 293 K, the dephasing model used throughout predicts coherence decay within only a few beat cycles. Lowering T reduces γ_ϕ approximately linearly in this fast-bath limit, suggesting a regime where many beat periods could be sustained and deterministic gates may become plausible.

As shown in Figure 4, the extrapolated half-lives already exceed the ~ 30 fs coherence half-life by two orders of magnitude, indicating that cryogenic operation could enable *many* coherent oscillations per gate.

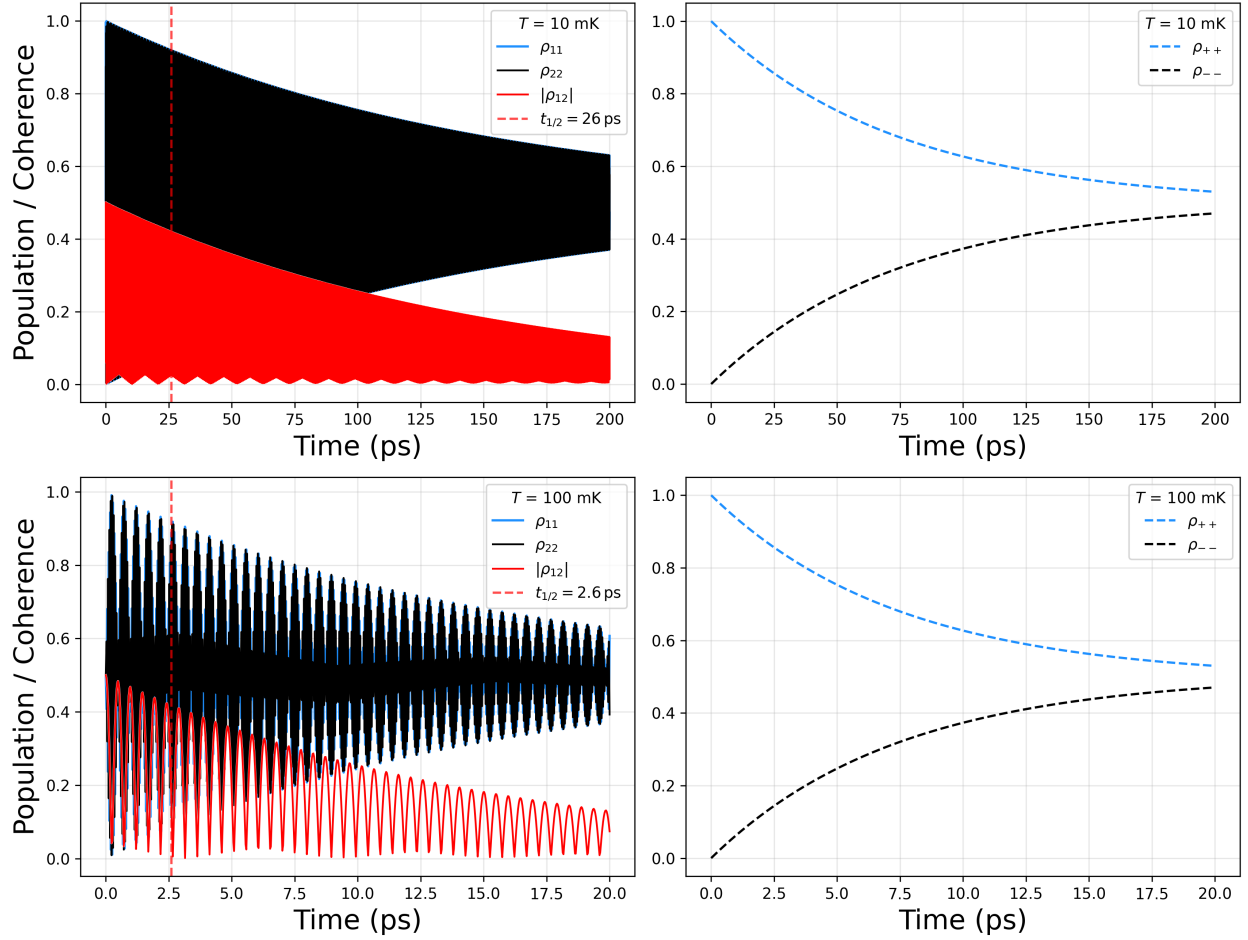


Figure 4: **Heuristic cryogenic-temperature extrapolation of coherence half-life.** The high-temperature dephasing model used throughout is heuristically extrapolated to cryogenic temperatures (10–100 mK). Although this violates the $k_B T \gg \hbar \omega_c$ assumption, it provides a *conservative lower bound*: true coherence half-lives $t_{1/2}$ would be longer than shown, since phonon populations are exponentially suppressed at low T . Even so, the extrapolation predicts $t_{1/2} \approx 2.6$ ps at 100 mK and $t_{1/2} \approx 26$ ps at 10 mK, placing FP dimers within a regime well-compatible with ultrafast optical gate times.

State-of-the-art cryogenic platforms already achieve electron temperatures in the 3–5 mK range on-chip via nuclear demagnetization [6], providing ample headroom to suppress dephasing if other material parameters remain favorable. While proteins are not nanoelectronic metals, this benchmark shows that the *temperature* regime needed to extend coherence by orders of magnitude is technically reachable. This invites exploration of hybrid photonic-biomolecular experiments that test FP dimers as near-room-temperature or cryogenic qubits with ultrafast optical control.

Current quantum computing context. State-of-the-art photonic quantum computers already rely on fs-to-ps pulsed lasers to define gate operations, with characteristic timescales well matched to excitonic beating in Venus-like dimers [34, 35]. Scaling to multi-qubit systems requires that coherence half-lives $t_{1/2}$ comfortably exceed gate times T_{gate} by at least an order of magnitude, so that errors do not accumulate catastrophically as qubit counts grow [32]. For FP-based qubits, this implies engineering conditions (temperature, geometry, environment) where $t_{1/2}/T_{\text{gate}} \gtrsim 10$.

Photonic vs. molecular qubits. Photonic qubits store information in polarization, frequency, or temporal modes, while molecular qubits rely on coherent superpositions of site or exciton states [33]. FP dimers sit naturally at the interface: dimerization defines a site/energy basis where excitonic coherence evolves, and emission occurs as polarized photons that can directly seed photonic quantum channels. Thus, Venus dimers provide a conceptual bridge between photonic and molecular approaches, with polarization anisotropy serving as a direct experimental handle on state preparation and readout [2, 36].

State preparation and design strategies. Coherent state preparation could be achieved by ultrafast resonant pumping of the bright exciton [21, 3], or by genetically engineering dimers biased toward the dark state such that emission is suppressed and coherence evolves “silently” until triggered. Two identical chromophores can be forced to couple with specific relative structural geometries to yield red- and blueshifted excitons (bright and dark states, respectively). Genetic variants that stabilize dark-favored manifolds may thus allow extended coherent evolution by evading radiative decay.

Forward-looking implications. The present analysis constrains the room-temperature limit (critical damping \Rightarrow effective single-emitter antibunching) and highlights how geometry and spectra tie to both functional and evolutionary constraints (including higher-order oligomerization). Moving forward, systematic exploration of regimes where $t_{1/2}$ can be extended—through temperature control, engineered rigidity, or targeted chromophore environments—will be essential for assessing whether FP dimers can achieve the $t_{1/2}/T_{\text{gate}}$ ratios needed for fault-tolerant operation. The same structural properties that evolution exploited for spectral tuning (chromophore geometry, protonation equilibria, oligomerization) may be repurposed as design principles for molecular qubits operating at the interface with photonic quantum technologies.

While Figure 4 extends the high-temperature dephasing model beyond its strict domain of validity, it provides a conservative benchmark. In practice, a rigorous low-temperature treatment would predict even longer coherence half-lives, further strengthening the case for hybrid photonic-biomolecular experiments at cryogenic temperatures. Hence, the same design tricks *Aequorea* jellyfish use to shine green in the ocean may one day be harnessed to keep qubits coherent in a quantum computer.

Conclusions

In this work, photon antibunching has been reconciled with strong excitonic coupling and absorption redshift in Venus YFP dimers. A Lindblad master equation model demonstrates that rapid dephasing suppresses quantum coherence in the presence of strong coupling, while thermal equilibration biases population into the bright excitonic state. Together, these mechanisms cause strongly coupled dimers to behave as bright single emitters, reconciling the apparent contradiction between strong coupling and antibunching. This connection constitutes the primary result.

Beyond this mechanistic reconciliation, the analysis links structural conservation in fluorescent proteins (FPs) to adaptive hypotheses and highlights the potential of FP dimers as candidate molecular qubits. More broadly, the results suggest that cryogenic cooling could extend coherence lifetimes into the regime required for quantum gate operations, while also revealing a deeper structural design principle—the “bioexciton motif.” This motif emphasizes how excitonic coupling, decoherence, and protein architecture act in concert not only to shape optical behavior but also to constrain and direct evolutionary adaptation. It offers a novel conceptual framework that could simplify future modeling efforts of similar chromoprotein systems

and bridge quantum technologies with evolutionary biology. Positioning excitonic structure as an adaptive motif thus provides both a mechanistic explanation for Venus YFP dimers and a guiding framework for experimental exploration and theoretical refinement across protein excitonics and quantum biophotonics.

Appendix

A Dynamics in a Drude-Lorentz Bath: Dephasing, Relaxation, and Effective Reorganization Energy

A.1 Pure Dephasing in the Energy Basis

Consider a system with Hamiltonian H_S that is linearly and diagonally coupled to a harmonic bath,

$$H = H_S + \sum_{\xi} \hbar \omega_{\xi} b_{\xi}^{\dagger} b_{\xi} + A \otimes \sum_{\xi} c_{\xi} (b_{\xi} + b_{\xi}^{\dagger}), \quad (6)$$

with $[H_S, A] = 0$. In the cumulant (Kubo) treatment for a Gaussian bath, the coherence between energy eigenstates $|+\rangle$ and $|-\rangle$ decays as [37, 10]

$$\rho_{+-}(t) = \rho_{+-}(0) e^{-i\omega_0 t} e^{-g(t)}, \quad g(t) = \int_0^t d\tau \int_0^{\tau} d\tau' C_{\omega}(\tau'), \quad (7)$$

where $C_{\omega}(t) = \langle \delta\omega(t) \delta\omega(0) \rangle$ with $\delta\omega(t) = \delta E(t)/\hbar$.

For a Drude-Lorentz spectral density

$$J(\omega) = \frac{2\lambda\omega\gamma_c}{\omega^2 + \gamma_c^2}, \quad (8)$$

the energy-gap correlation function is

$$C_E(t) = \lambda\gamma_c \left[\cot\left(\frac{\beta\hbar\gamma_c}{2}\right) - i \right] e^{-\gamma_c t} + \text{Matsubara terms}. \quad (9)$$

In the classical/high- T limit, Matsubara terms can be neglected and

$$C_{\omega}(t) = \frac{1}{\hbar^2} \text{Re } C_E(t) \simeq \frac{2\lambda k_B T}{\hbar^2} e^{-\gamma_c t}. \quad (10)$$

The lineshape function evaluates to

$$g(t) = \frac{2\lambda k_B T}{\hbar^2} \left[\frac{t}{\gamma_c} - \frac{1 - e^{-\gamma_c t}}{\gamma_c^2} \right], \quad (11)$$

with limits

$$g(t) \simeq \frac{\lambda k_B T}{\hbar^2} t^2 \quad (t \ll \tau_c), \quad g(t) \simeq \frac{2\lambda k_B T}{\hbar^2 \gamma_c} t \quad (t \gg \tau_c).$$

Thus, in the motional-narrowing limit the pure-dephasing rate is

$$\boxed{\gamma_{\phi} = \frac{2\lambda k_B T}{\hbar^2 \gamma_c}} \quad (12)$$

Remark on correlation time. Where the single-Debye Drude-Lorentz form [Eq. (12)] is invoked, we adopt a conservative correlation time $\tau_c = 0.1$ ps. This ensures that the motional-narrowing condition $\tau_c \ll T_2$ is firmly satisfied, which maximally simplifies the Bloch-Redfield treatment while still remaining consistent with the observed picosecond coherence times. In this sense, $\tau_c = 0.1$ ps should be viewed as a pragmatic modeling parameter chosen to keep the analytic form tractable, rather than as a literal microscopic estimate of the bath memory time.

A.2 Rotation to the Site Basis

Transforming from the excitonic basis to the site basis introduces off-diagonal coherences that couple site populations through the delocalized eigenstates. For a site-energy difference Δ (Stokes shift) and coupling J , the Hamiltonian in the site basis is hence

$$H = \begin{bmatrix} -\Delta/2 & J \\ J & +\Delta/2 \end{bmatrix}. \quad (13)$$

Diagonalization yields eigenenergies $E_{\pm} = \bar{\varepsilon} \pm \frac{1}{2}\Delta E$, where $\Delta E = \sqrt{\Delta^2 + 4J^2}$. In this representation, population relaxation and dephasing are controlled by γ_{ϕ} together with the thermal transfer rates γ_{+-} and γ_{-+} , which redistribute exciton populations according to detailed balance. This site-basis perspective is essential for analyzing relaxation pathways following structural or solvent-induced energy shifts.

A.3 Thermal Population Transfer (Born-Markov-secular Limit)

Within the Born-Markov-secular approximation, thermal transitions between excitonic states are described by downhill (γ_{-+}) and uphill (γ_{+-}) rates. These follow from Fermi’s golden rule applied to the bath spectral density, with detailed balance ensuring

$$\frac{\gamma_{+-}}{\gamma_{-+}} = e^{-\beta\Delta E}, \quad (14)$$

where ΔE is the exciton splitting and $\beta = 1/(k_B T)$. The downhill rate γ_{-+} is set by the overlap of the spectral density with the excitonic transition frequency, while the uphill rate γ_{+-} is exponentially suppressed at low temperature. Together with the pure-dephasing rate γ_{ϕ} , these thermal rates define the full Lindblad dynamics of the dimer, governing both relaxation into the bright state and the loss of coherence between excitons.

A.4 Effective Reorganization Energy from Experimental Coherence Times

Cinelli *et al.* reported room-temperature coherent dynamics in GFP with a *dephasing time of about 1 ps* [11]. Following Burgess and Florescu’s double-Debye dielectric model for the GFP chromophore pocket (cavity geometry plus two solvent relaxation channels), the pure-dephasing rate obeys the general Bloch-Redfield relation

$$\gamma_{\phi} = \pi T \lim_{\omega \rightarrow 0} \frac{J(\omega)}{\omega}, \quad (15)$$

with $T \equiv k_B T/(hc) \approx 208 \text{ cm}^{-1}$ at 293 K.

Evaluating this expression with $T_2 \approx 1 \text{ ps}$ as the observed coherence time and using the double-Debye spectral density yields an effective reorganization energy

$$\boxed{\lambda \approx 2.7 \times 10^2 \text{ cm}^{-1}} \quad (16)$$

consistent with the picosecond-scale dynamics reported by Cinelli *et al.*

Conflict of Interest

The author declares no conflict of interest.

Acknowledgments

The author acknowledges use of the QuTiP framework (v5.2.0) [12, 13] for open quantum system simulations, NumPy (v2.3.2) [14] for array programming and scientific computing, SciPy (v1.16.0) [15] for scientific algorithms and numerical routines, and open-source PyMOL (v2.5, commit d24468af) [25] for molecular graphics.

I am grateful to Y. Kim for welcoming me as a PhD student and for granting the intellectual freedom to pursue the subjects presented in this work. I am also grateful to A. Rocco for introducing me to the world of theoretical physics research and to A. P. Kalra for encouraging me to pursue my own ideas.

I additionally thank several faculty members at Ursinus College for supporting my diverse interests and, in particular, R. Martin-Wells for keeping me on my toes throughout PHYS-207W (Modern Physics), where my foundation in quantum physics was originally built.

Funding

This research received no external funding and was conducted using the author’s own time and computational resources.

Code and Data Availability

All figure scripts, the conda environment, and supporting materials required to reproduce this work are archived on Zenodo, version v1.2.0-arxiv (DOI: 10.5281/zenodo.16892071) [38] and mirrored on GitHub (<https://github.com/ianthomasabrahams/venus-dimer-theory-figures>).

References

- [1] Albert Einstein. *Investigations on the Theory of the Brownian Movement*. Dover Publications, New York, 1956. English translation of Einstein’s 1905 paper: “Über die von der molekularkinetischen Theorie der Wärme geforderte Bewegung von in ruhenden Flüssigkeiten suspendierten Teilchen,” *Annalen der Physik* 17, 549–560 (1905).
- [2] Youngchan Kim, Henry L. Puhl, Eefei Chen, Grace H. Taumoefolau, Tuan A. Nguyen, David S. Kliger, Paul S. Blank, and Steven S. Vogel. Venus₂₀₆ dimers behave coherently at room temperature. *Biophysical Journal*, 116(10):1918–1930, 2019.
- [3] Youngchan Kim, Federico Bertagna, Edeline M. D’Souza, Derren J. Heyes, Linus O. Johannissen, Evelyn T. Nery, Antonio Pantelias, Alejandro Sanchez-Pedreño Jimenez, Louie Slocombe, Michael G. Spencer, Jim Al-Khalili, Gregory S. Engel, Sam Hay, Suzanne M. Hingley-Wilson, Kamalan Jeevaratnam, Alex R. Jones, Daniel R. Kattnig, Rebecca Lewis, Marco Sacchi, Nigel S. Scrutton, S. Ravi P. Silva, and Johnjoe McFadden. Quantum biology: An update and perspective. *Quantum Reports*, 3(11):80–126, 2021.
- [4] Priyankar Banerjee, Adam Burgess, Julian Wiercinski, Moritz Cygorek, and Erik M. Gauger. Optical signatures of coherence in molecular dimers. *arXiv preprint arXiv:2505.13435*, 2025.
- [5] Adam Burgess and Marian Florescu. Dynamical decoherence and memory effects in green fluorescent proteins by dielectric relaxation. *arXiv preprint arXiv:2211.09408*, 2024.
- [6] Nikolai Yurttagül, Matthew Sarsby, and Attila Geresdi. Indium as a high-cooling-power nuclear refrigerant for quantum nanoelectronics. *Physical Review Applied*, 12(1):011005, 2019.
- [7] V. May and O. Kühn. *Molecular Physics: Theoretical Principles and Experimental Methods*. Wiley-VCH, Weinheim, 2011.
- [8] Gregory D. Scholes. Long-range resonance energy transfer in molecular systems. *Annual Review of Physical Chemistry*, 54(1):57–87, 2003.
- [9] Gregory D. Scholes. Polaritons and excitons: Hamiltonian design for enhanced coherence. *Proceedings of the Royal Society A: Mathematical, Physical and Engineering Sciences*, 476(2242):20200278, 2020.
- [10] Heinz-Peter Breuer and Francesco Petruccione. *The Theory of Open Quantum Systems*. Oxford University Press, Oxford, UK, 2002.

- [11] Riccardo A. G. Cinelli, Valentina Tozzini, Vittorio Pellegrini, Fabio Beltram, Giulio Cerullo, Margherita Zavelani-Rossi, Sandro De Silvestri, Mudit Tyagi, and Mauro Giacca. Coherent dynamics of photoexcited green fluorescent proteins. *Physical Review Letters*, 86(15):3439–3442, 2001.
- [12] J. R. Johansson, P. D. Nation, and F. Nori. Qutip: An open-source python framework for the dynamics of open quantum systems. *Computer Physics Communications*, 183(8):1760–1772, 2012.
- [13] J. R. Johansson, P. D. Nation, and F. Nori. Qutip 2: A python framework for the dynamics of open quantum systems. *Computer Physics Communications*, 184(4):1234–1240, 2013.
- [14] Charles R. Harris, K. Jarrod Millman, Stéfan J. van der Walt, Ralf Gommers, Pauli Virtanen, David Cournapeau, Eric Wieser, Julian Taylor, Sebastian Berg, Nathaniel J. Smith, Robert Kern, Matti Picus, Stephan Hoyer, Marten H. van Kerkwijk, Matthew Brett, Allan Haldane, Jaime Fernández del Río, Mark Wiebe, Pearu Peterson, Pierre Gérard-Marchant, Kevin Sheppard, Tyler Reddy, Warren Weckesser, Hameer Abbasi, Christoph Gohlke, and Travis E. Oliphant. Array programming with NumPy. *Nature*, 585(7825):357–362, 2020.
- [15] Pauli Virtanen, Ralf Gommers, Travis E. Oliphant, Matt Haberland, Tyler Reddy, David Cournapeau, Evgeni Burovski, Pearu Peterson, Warren Weckesser, Jonathan Bright, Stéfan J. van der Walt, Matthew Brett, Joshua Wilson, K. Jarrod Millman, Nikolay Mayorov, Andrew R. J. Nelson, Eric Jones, Robert Kern, Eric Larson, C. J. Carey, İlhan Polat, Yu Feng, Eric W. Moore, Jake VanderPlas, Denis Laxalde, Josef Perktold, Robert Cimrman, Ian Henriksen, E. A. Quintero, Charles R. Harris, Anne M. Archibald, Antônio H. Ribeiro, Fabian Pedregosa, Paul van Mulbregt, and SciPy 1.0 Contributors. SciPy 1.0: Fundamental algorithms for scientific computing in python. *Nature Methods*, 17:261–272, 2020.
- [16] Robert M. Clegg. Fluorescence resonance energy transfer: Fret what is it, why do it, and how it’s done. *Laboratory Techniques in Biochemistry and Molecular Biology*, 33:1–57, 1996.
- [17] Gregory D. Scholes, Xanthipe J. Jordanides, and Graham R. Fleming. Adapting the förster theory of energy transfer for modeling dynamics in aggregated molecular assemblies. *The Journal of Physical Chemistry B*, 105(8):1640–1651, 2001.
- [18] Nancy Makri. Numerical path integral techniques for long-time quantum dynamics of dissipative systems. *The Journal of Chemical Physics*, 102(11):4600–4610, 1995.
- [19] Hans Martin Senn and Walter Thiel. Qm/mm methods for biomolecular systems. *Angewandte Chemie International Edition*, 48(7):1198–1229, 2009.
- [20] Akihito Ishizaki and Graham R. Fleming. Unified treatment of quantum coherent and incoherent hopping dynamics in electronic energy transfer: Reduced hierarchy equation approach. *The Journal of Chemical Physics*, 130(23):234111, 2009.
- [21] Gregory S. Engel, Travis R. Calhoun, Elizabeth L. Read, Tessa-Kay Ahn, Tomas Mancal, Yuan-Chung Cheng, Robert E. Blankenship, and Graham R. Fleming. Evidence for wavelike energy transfer through quantum coherence in photosynthetic systems. *Nature*, 446:782–786, 2007.
- [22] Shuo Wang, Zhen Li, Baoxia Ding, Dong Liang, and Kai Xu. Single-molecule imaging and computational microscopy approaches clarify the mechanism of the dimerization of human neurotensin receptor 1. *Journal of the American Chemical Society*, 141(8):3146–3155, 2019.
- [23] Markus Wendling, Milosz A. Przyjalowski, Demet Gülen, Simone I. E. Vulto, Thijs J. Aartsma, Rienk van Grondelle, and Herbert van Amerongen. The quantitative relationship between structure and polarized spectroscopy in the fmo complex of *Prosthecochloris aestuarii*: refining experiments and simulations. *Photosynthesis Research*, 71(1–2):99–123, 2002.
- [24] T. Pullerits and V. Sundström. Photosynthetic light-harvesting: Reconciling dynamics and structure of purple bacterial lh2 reveals function of photosynthetic unit. *Accounts of Chemical Research*, 32(7):479–486, 1999.

- [25] Schrödinger, LLC. Pymol open-source molecular graphics system (v2.5, commit d24468af). <https://github.com/schrodinger/pymol-open-source>, 2021.
- [26] Gerard G. Lambert, Hadrien Depernet, Guillaume Gotthard, Darrin T. Schultz, Isabelle Navizet, Talley Lambert, Stephen R. Adams, Albertina Torreblanca-Zanca, Meihua Chu, Daphne S. Bindels, Vincent Levesque, Jennifer Nero Moffatt, Anya Salih, Antoine Royant, and Nathan C. Shaner. Aequorea’s secrets revealed: New fluorescent proteins with unique properties for bioimaging and biosensing. *PLOS Biology*, 18(11):e3000936, 2020.
- [27] Nathan C. Shaner. Imaging data for lambert et al, aequorea’s secrets revealed: new fluorescent proteins with unique properties for bioimaging and biosensing, 2020.
- [28] Bella L. Grigorenko, Alexander V. Nemukhin, Igor V. Polyakov, Dmitry I. Morozov, and Anna I. Krylov. First-principles characterization of the energy landscape and optical spectra of green fluorescent protein along the a \rightarrow i \rightarrow b proton transfer route. *Journal of the American Chemical Society*, 135(31):11541–11549, August 2013.
- [29] Andrey Yu. Gorokhovatsky, Victor V. Marchenkov, Natalia V. Rudenko, Tanya V. Ivashina, Vladimir N. Ksenzenko, Nils Burkhardt, Gennady V. Semisotnov, Leonid M. Vinokurov, and Yuli B. Alakhov. Fusion of *Aequorea victoria* gfp and aequorin provides their ca²⁺-induced interaction that results in red shift of gfp absorption and efficient bioluminescence energy transfer. *Biochemical and Biophysical Research Communications*, 320(3):703–711, 2004.
- [30] Mark A. Wall, Michael Socolich, and Rama Ranganathan. The structural basis for red fluorescence in the tetrameric gfp homolog dsred. *Nature Structural Biology*, 7(12):1133–1138, 2000.
- [31] Nathan C. Shaner, Gerard G. Lambert, Andrew Chammas, Yuhui Ni, Paula J. Cranfill, Michelle A. Baird, Brittney R. Sell, John R. Allen, Richard N. Day, Maria Israelsson, Michael W. Davidson, and Jiwu Wang. A bright monomeric green fluorescent protein derived from branchiostoma lanceolatum. *Nature Methods*, 10(5):407–409, 2013.
- [32] John Preskill. Reliable quantum computers. *Proceedings of the Royal Society of London. Series A: Mathematical, Physical and Engineering Sciences*, 454(1969):385–410, 1998.
- [33] Michael A. Nielsen and Isaac L. Chuang. *Quantum Computation and Quantum Information*. Cambridge University Press, Cambridge, 10th anniversary edition edition, 2010.
- [34] Jeremy L. O’Brien. Optical quantum computing. *Science*, 318(5856):1567–1570, 2007.
- [35] Fulvio Flamini, Nicolò Spagnolo, and Fabio Sciarrino. Photonic quantum information processing: a review. *Reports on Progress in Physics*, 82(1):016001, 2018.
- [36] R. Jiménez and colleagues. Ultrafast fluorescence depolarisation in green fluorescence protein tandem dimers as hydrophobic environment sensors. *Chemical Science*, 14(36):10677–10685, 2023.
- [37] Ryogo Kubo. The fluctuation-dissipation theorem. *Reports on Progress in Physics*, 29(1):255–284, 1966.
- [38] Ian T. Abrahams. Zenodo figures for excitonic coupling in venus dimers. <https://doi.org/10.5281/zenodo.16892071>, 2025. Accessed: 2025-08-18.